GEOPHYSICS, VOL. 73, NO. 3 (MAY-JUNE 2008); P. F105–F113, 9 FIGS.
10.1190/1.2895521

Quasi-3D modeling of airborne TEM data by spatially constrained inversion

Andrea Viezzoli[1], Anders Vest Christiansen[1], Esben Auken[1], and Kurt Sørensen[1]

ABSTRACT

We present a new methodology, spatially constrained inversion (SCI), that produces quasi-3D conductivity modeling of electromagnetic (EM) data using a 1D forward solution. Spatial constraints are set between the model parameters of nearest neighboring soundings. Data sets, models, and spatial constraints are inverted as one system. The constraints are built using Delaunay triangulation, which ensures automatic adaptation to data density variations. Model parameter information migrates horizontally through spatial constraints, increasing the resolution of layers that would be poorly resolved locally. SCI produces laterally smooth results with sharp layer boundaries that respect the 3D geological variations of sedimentary settings. SCI also suppresses the elongated artifacts commonly seen in interpretation results of profile-oriented data sets. In this study, SCI is applied to airborne time-domain EM data, but it can also be implemented with other ground-based or airborne data types.

INTRODUCTION

Airborne electromagnetic (AEM) surveys conducted around the globe produce hundreds of thousands of line-kilometers of data every year. Because of the enormous computational costs involved in a full nonlinear 3D inversion, these data are usually inverted using a 1D forward model. The 1D model assumption is legitimate in quasi-layered sedimentary areas, where it produces results only slightly distorted by 2D or 3D effects (Newman et al., 1987; Sengpiel and Siemon, 2000; Auken et al., 2005a). In some cases, the resulting models are stitched together (Macnae and Lamontagne, 1987; Auken et al., 2003; Huang and Fraser, 2003), often resulting in abrupt variations in neighboring models because of inherently noisy data and model equivalence. This is a nonoptimal result for sedimentary environments where the lateral variations are expected to be smooth. Models with smooth lateral variations can be achieved by working in either the data domain or the model domain.

The first approach, which is widely used with both frequency- and time-domain airborne EM data, entails smoothing the raw data before inversion. In this case, the signal-to-noise ratio is increased at the cost of decreasing lateral resolution. In the second approach, the constraints are applied between adjacent models during the inversions and the data require less smoothing, thus keeping the detailed earth information in the data. Examples of inversion methodologies that constrain the models are the laterally constrained inversion (LCI) of galvanic (Auken and Christiansen, 2004) and EM data (Santos, 2004; Auken et al., 2005b; Mansoor et al., 2006) and the simultaneous inversion method of galvanic data (Gyulai and Ormos, 1999).

Each of these processing or inversion techniques is profile oriented, in the sense that they aim at producing a continuum along a line. However, they do not create any connection between neighboring lines. Features that are perpendicular to flight lines benefit only partially from inline constraints or smoothing because no information in the model space is passed between adjacent lines. This means that profile-oriented techniques favor structures following the flight direction. Producing spatial maps based on such methodologies often results in some lineation following the flight paths.

In this paper, we expand the concept of along-profile LCI to spatially constrained inversion (SCI), which operates both along and across profiles. The principles of SCI are similar to those of LCI, the only difference being in the constraints, which are set laterally in two dimensions rather than just laterally along the flight line. Being an overdetermined problem, a full sensitivity analysis of the output models is produced, allowing a quantitative evaluation of the inversion results.

SCI has some similarity with the quasi-3D layered inversion methodology presented by Brodie and Sambridge (2006). Their algorithm is specially designed for helicopter electromagnetic (HEM) data. By using bicubic B-splines, they invert a 3D grid (using a 1D forward solution) for a combination of layered-earth parameters and

Manuscript received by the Editor 24 May 2007; revised manuscript received 18 December 2007; published online 11 April 2008.
[1]University of Aarhus, Department of Earth Sciences, Aarhus, Denmark. E-mail: andrea.viezzoli@geo.au.dk; anders.vest@geo.au.dk; esben.auken@geo.au.dk; kurt.sorensen@geo.au.dk.

gain-phase and bias parameters related to the calibration of the HEM data. Their solution is formulated using sparse matrix solvers, which enable them to invert extremely large data sets without dividing them into subsets. The grid cells are often rectangular, with significantly fewer node locations than observations, as opposed to SCI, which, as we discuss, is based on actual observation locations.

In the next section, we describe the SCI concept. Then we show its results on a data set of airborne time-domain EM (TEM) data, both in the form of average resistivity slices maps and of resistivity section profiles. We compare the results of SCI with stitched-together single-site inversions and LCI.

SCI METHODOLOGY

The mathematical formulation of the SCI method is very similar to that of the LCI method (Auken and Christiansen, 2004). It is a least-squares inversion of a layered earth regularized through spatial constraints, which give smooth lateral transitions. Model parameter information from areas with well-resolved parameters migrates through the constraints to help resolve areas with poorly constrained parameters. Similarly, a priori information, used to resolve ambiguities and to add, for example, geologic information, can be added at any point of the profile. It then migrates through the lateral constraints to parameters at adjacent sites. In noisy soundings, the spatial constraints help to resolve model parameters using the information coming from the neighboring soundings.

Lateral constraints can be applied to any model parameter. Our approach is to constrain layer resistivity and either layer boundary thickness or depth. Constraints on depths are often preferred over constraints on thickness, especially in sedimentary settings, because the models produced display higher horizontal continuity. Constraints on thickness are more suitable in the presence of layer-boundary discontinuities (e.g., a fault).

The dependence of apparent resistivity on subsurface parameters is generally described as a nonlinear differentiable forward mapping. For data inversion, we follow the established practice of linearized approximation by the first term of the Taylor expansion:

$$\mathbf{d}_{\text{obs}} - \mathbf{e}_{\text{obs}} \cong \mathbf{G}\delta\mathbf{m}_{\text{true}} + \mathbf{g}(\mathbf{m}_{\text{ref}}), \tag{1}$$

where $\mathbf{d}_{\text{obs}}$ is the observed data, $\mathbf{e}_{\text{obs}}$ is the error on the observed data, $\mathbf{g}$ is the nonlinear mapping of the model to the data space, and $\delta\mathbf{m}_{\text{true}} = \mathbf{m}_{\text{true}} - \mathbf{m}_{\text{ref}}$. The true model $\mathbf{m}_{\text{true}}$ must be sufficiently close to some arbitrary reference model $\mathbf{m}_{\text{ref}}$ for the linear approximation to be valid. We choose to apply logarithmic parameters to minimize nonlinearity and impose positivity.

The Jacobian matrix $\mathbf{G}$ contains the partial derivatives of the mapping:

$$\mathbf{G}_{ab} = \frac{\partial \mathbf{d}_a}{\partial \mathbf{m}_b} \tag{2}$$

for the ath datum and the bth model parameter.

In short, we write

$$\mathbf{G}\delta\mathbf{m}_{\text{true}} = \delta\mathbf{d}_{\text{obs}} - \mathbf{e}_{\text{obs}}, \tag{3}$$

where $\delta\mathbf{d}_{\text{obs}} = \mathbf{d}_{\text{obs}} - \mathbf{g}(\mathbf{m}_{\text{ref}})$.

The constraints are connected to the true model as

$$\mathbf{R}\delta\mathbf{m}_{\text{true}} = \delta\mathbf{r} + \mathbf{e}_r, \tag{4}$$

where $\mathbf{e}_r$ is the error on the constraints, with zero as the expected value. The term $\delta\mathbf{r} = -\mathbf{R}\mathbf{m}_{\text{ref}}$ claims identity between the parameters tied by constraints in the roughening matrix $\mathbf{R}$. The main difference between SCI and LCI is in the entries of $\mathbf{R}$. In LCI, only constraints on neighboring along-line soundings (i.e., soundings along a flight line or a profile) are included, and $\mathbf{R}$ contains 1 and -1 for the constrained parameters:

$$\mathbf{R} = \begin{bmatrix} 1 & 0 & \cdots & 0 & -1 & 0 & \cdots & 0 & 0 & 0 \\ 0 & 1 & 0 & \cdots & 0 & -1 & 0 & \cdots & 0 & 0 \\ \vdots & & & & & \vdots & & & & \vdots \\ 0 & 0 & 0 & \cdots & 0 & 1 & 0 & \cdots & 0 & -1 \end{bmatrix}. \tag{5}$$

In SCI, the constraints are also applied to offline soundings so each model parameter is connected to many other model parameters of the same kind (e.g., resistivity of layer 2 with resistivity of other layer 2s from constrained soundings). The roughening matrix for SCI is

$$\mathbf{R} = \begin{bmatrix} N^1 & 0 & \cdots & 0 & -1 & 0 & \cdots & 0 & -1 & 0 & \cdots & 0 & 0 & 0 \\ 0 & N^2 & 0 & \cdots & 0 & -1 & 0 & \cdots & 0 & -1 & 0 & \cdots & 0 & 0 \\ \vdots & & & & & & & \vdots & & & & \vdots & & \\ 0 & 0 & 0 & \cdots & 0 & N^j & 0 & \cdots & 0 & -1 & 0 & \cdots & 0 & -1 \end{bmatrix}, \tag{6}$$

where N^j is the number of models that the jth model parameter is constrained to. For the jth row, $|\Sigma(-1)| = N^j$. In both LCI and SCI, $\mathbf{R}$ is sparse so that sparse operations can be applied. The variance, or strength of the constraints, is described in the covariance matrix $\mathbf{C}_{\mathbf{R}}$, which has nonzero entries in the same locations of $\mathbf{R}$.

By joining equations 3 and 4, we can write the inversion problem as

$$\begin{bmatrix} \mathbf{G} \\ \mathbf{R} \end{bmatrix} \cdot \delta\mathbf{m}_{\text{true}} = \begin{bmatrix} \delta\mathbf{d}_{\text{obs}} \\ \delta\mathbf{r} \end{bmatrix} + \begin{bmatrix} \mathbf{e}_{\text{obs}} \\ \mathbf{e}_{\mathbf{r}} \end{bmatrix}, \tag{7}$$

or, more compactly,

$$\mathbf{G}' \cdot \delta\mathbf{m}_{\text{true}} = \delta\mathbf{d}' + \mathbf{e}'. \tag{8}$$

The covariance matrix for the joint observation error $\mathbf{e}'$ becomes

$$\mathbf{C}' = \begin{bmatrix} \mathbf{C}_{\text{obs}} & \underline{0} \\ \underline{0} & \mathbf{C}_R \end{bmatrix}, \tag{9}$$

where $\mathbf{C}_{\text{obs}}$ refers to the observational errors $\mathbf{e}_{\text{obs}}$ and $\mathbf{C}_R$ refers to the error on the constraints $\mathbf{e}_r$. If a priori data are present, another row is added to equation 9.

The objective function, with ND as the number of data and NC the number of constraints, is

$$Q = \left(\frac{1}{ND + NC} [(\delta\mathbf{d}'^T \mathbf{C}'^{-1} \delta\mathbf{d}')] \right)^{1/2}; \tag{10}$$

the objective function is minimized by

$$\delta\mathbf{m}_{\text{est}} = (\mathbf{G}'^T \mathbf{C}'^{-1} \mathbf{G}')^{-1} \mathbf{G}'^T \mathbf{C}'^{-1} \delta\mathbf{d}'. \tag{11}$$

This implies that the data misfit and the model roughness (i.e., the constraints) are minimized. In LCI, only along-line soundings are

included in the objective function. In SCI, the function includes also offline soundings.

The forward 1D calculation is based on the solutions in Ward and Hohmann (1988). The transmitter is modeled by integrating horizontal electric dipoles along the wire path. A low-pass filter (Effersø et al., 1999) is applied in the frequency domain, whereas transmitter waveform, instrument front-gate, and low-pass filters following the front gate are applied by convolution directly in the time domain. The frequency to time-domain transform is done using a cosine or sine transform with digital filters.

Conceptually, there are three main steps in SCI. The first is to select constraining points with Delaunay triangulation. We complete a Delauney triangulation on the whole data set. For each data point, we identify the immediate nearest neighbors that will be used to constrain model parameters.

The second step is to perform the first inversion run on large data subsets suitable for parallel computation. We identify subsets, herein called cells, that will be inverted independently. Using the Delauney triangulation results to iteratively expand membership of cells, we start with the nearest neighbors of a random point, add their nearest neighbors, and so on, until a fixed number of points is reached. Adjacent cells overlap by one rank of nearest neighbors. For each cell, we complete an independent SCI.

Finally, we preserve continuity across subsets with a second inversion run, repeating the inversion using the first inversion results as starting models and/or a priori information for the second inversion. In the following sections, we expand upon each of these points separately.

Selecting constraining points with Delaunay triangulation

The first step for constraining soundings that cover an area is to choose a strategy for connecting them. Such connections need to be repeatable, not arbitrary, and adapt as much as possible to the spatial distribution of the data set. In our approach, we use the Delaunay triangulation for this purpose.

The Delaunay triangulation is the 2D version of the more general 3D Delaunay tessellation, which has been widely applied in different areas of research as a favored method of representing surfaces and reconstructing 3D objects. For a detailed description of Delaunay tessellation, see Aurenhammer (1991). In geophysics, Delaunay triangulation has been applied to seismic tomography (Bohm et al., 2000), to integrating data for reconstructing 3D objects (Xue et al., 2004), for interpolating irregular data sets (Sambridge et al., 1995), and in parameter-searching algorithms (Sambridge, 1999).

Given a set of n points in a plane, $S_1(x,y), S_2(x,y), \ldots, S_n(x,y)$, with S_n being the point (or sounding) n, Delaunay triangulation represents the only way to triangulate them so that all points in the set that do not belong to a given triangle are external to the circumcircle of that triangle. This means the points at the vertices of the given triangle are nearest neighbors. An example of Delaunay triangulation is given in Figure 1. Note the points are included in a convex polygon and each is connected to at least three others.

An important characteristic of Delaunay triangles is that they vary in dimension according to the local data density. They adapt to the density of the data set, so they are small and numerous in high-density areas but large and fewer in low-density areas. The number of connections to each sounding is not set arbitrarily but depends on data density and distribution. Figure 2b shows the Delaunay triangulation of a set of 5477 SkyTEM (Sørensen and Auken, 2004) soundings recorded in the Stevnstrup area, eastern Jutland, Denmark (Figure 2a). Delaunay triangulation connects at least two adjacent lines, which is required if flight-line artifacts in the conductivity model are to be removed. Figure 2c shows the frequency histogram of the number of connections between soundings. On average, each sounding is linked to six other soundings, with a minimum of three and a maximum of 18 connections.

The second step for setting the constraints is to decide how many neighboring soundings each sounding should be constrained to. We decided to set the constraint between the nearest neighbors, i.e., between the soundings connected by Delaunay triangles (see Figure 3a). This way, each sounding (in this case sounding a) is linked to its best companions, i.e., the nearest neighbors (soundings b-g). They, in turn, are constrained to their nearest neighbors (soundings a-w, Figure 3b), and so on. The result is a continuum of interconnected soundings, each of which is only constrained to its nearest neighbor. Model parameter information spreads horizontally between nearest neighbors and then to the whole data set.

There are a number of different algorithms for calculating the Delaunay triangulation. We adopt the Quickhull algorithm (Barber et al., 1996). Carrying out the Delaunay triangulation with this algorithm takes an insignificant amount of time (for this data set, less than a second). It is important to notice that, even though the Delaunay triangles are used in more than one stage of the SCI, the triangulation of all data points is performed only once.

As mentioned above, the lateral constraints can be set for any model parameter. Our approach is to constrain layer resistivities and layer boundary depths.

The third and final step in preparing the constraints is setting their strength, which is described in the covariance matrix C_R. The constraints need to reflect the expected variations in the geologic model. In SCI, as in LCI, this is achieved empirically by means of model recognition analysis and subsequent trial and error fine-tuning. The constraints applied are to a large degree based on studies of 3D forward modeling of complicated geologic models followed by LCI (Auken et al., 2005b; E. Auken et al., personal communication, 2008). The strength of the constraints is distance dependent, as shown in equation 12:

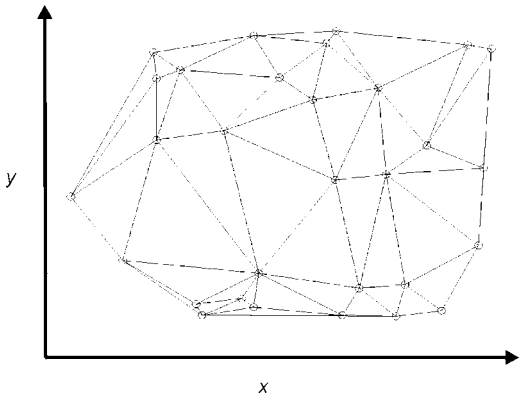

Figure 1. Delaunay triangulations of a randomly generated set of points on a plane.

$$C\_\mathrm{SCI}(d) = 1 + (A - 1)\left(\frac{d}{B}\right)^{a}, \qquad (12)$$

where d represents the distance between two constrained soundings, B the reference distance, and A the reference constraint value. The reference distance is the typical separation between adjacent soundings, and the reference constraint is the value to which the strength of the constraints is set in case of soundings that are closer than the reference distance. The exponent a determines how the constraints loosen up with distance (e.g., linearly, for $a = 1$).

In this case, we used $A = 1.4$, $B = 40$ m, and $a = 1.5$. According to our experience, the output of the inversion is reliably robust with respect to a wide range of choices for these parameters.

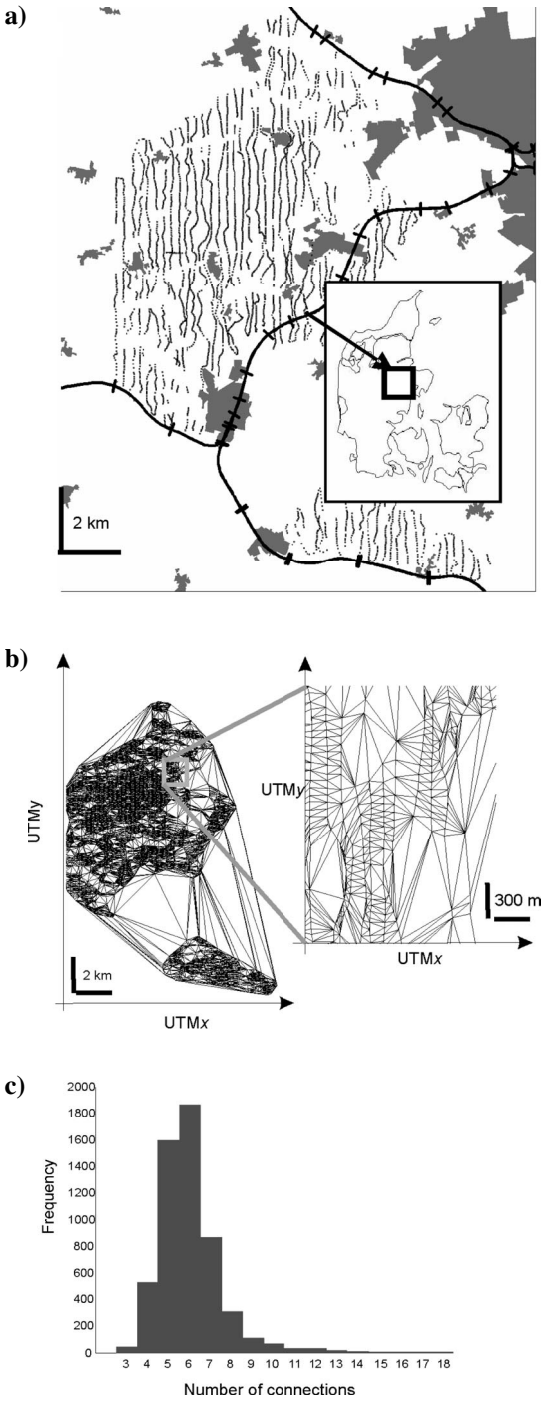

Figure 2. (a) The Stevnstrup field area. The map area is approximately 290 km^2. Each dot represents a sounding. (b) Delaunay triangulation of more than 1000 skyTEM soundings from the Stevenstrup area. (c) Frequency histogram of the number of connections between soundings in the Delaunay triangulation.

Performing the first inversion run on large subsets suitable for parallel computation

Implementation of SCI uses a Cholezski decomposition with back substitution with, currently, nonsparse matrix operations. This causes a computational limitation when inverting the Jacobian matrix $\mathbf{G}'$ in equation 11. Therefore, a typical data set of thousands of soundings must be divided into smaller subsets. Each subset is then inverted with spatial constraints as a unit. If the number of model parameters contained in a subset is about 1000, the time spent doing the Cholezski decomposition is comparable to the time spent calculating the Jacobian matrix.

For a five-layer model, 1000 model parameters are equivalent to about 100 soundings. The SCI is completed on 100 SkyTEM soundings in about 15 minutes. A single SkyTEM sounding is inverted, on a 64-bit, 2-GHz processor, in about 5 s using a very conservative regularization and starting from a half-space model. One hundred individual soundings without constraints take about 10 minutes. The SCI is, therefore, about 50% slower than the collection of single-site inversions.

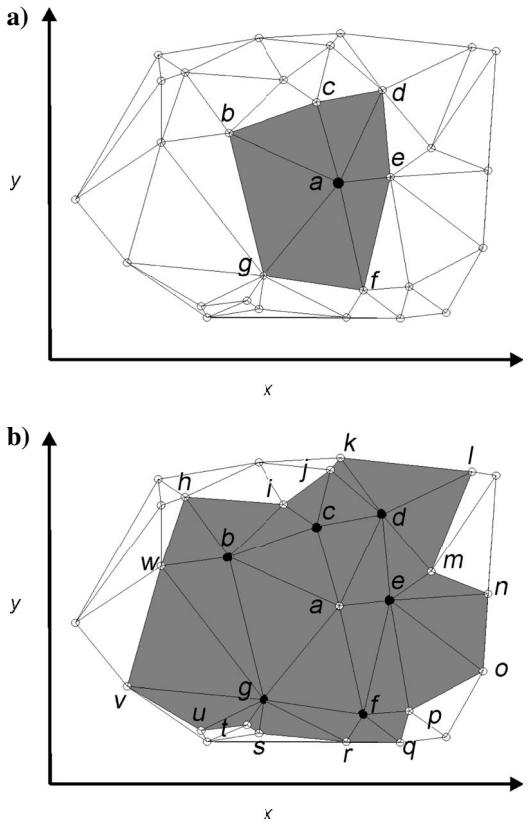

Figure 3. Delaunay-controlled progression of connections between nearest neighbors. (a) Sounding a is first connected to soundings b-g. (b) Soundings b-g are then connected to their nearest neighbors, h-w, creating a continuum of interconnected soundings.

If, for the purpose of defining the subsets, we superimpose on the entire data set predefined cells of given sizes and shapes, the density of the soundings in such cells could vary drastically because of the varying data density of the whole data set. This would decrease CPU efficiency. Instead, we once again turn to the Delaunay triangulation, which allows the construction of geometrically unbiased subsets of data that adapt automatically to data-density variations.

Cell construction is a multistep process. We select a starting point randomly and then identify its nearest neighbors, as defined above. They produce an outer border around the staring point (Figure 3a). Then we identify the neighbors nearest to each of the points along the border. This way, the cell is expanded to the next order of nearest neighbors. We keep expanding the cell by selecting the nearest neighbors to the points along the border of the previous iteration until a predefined number of points is included in the cell. For a five-layer model, that means approximately 100 soundings per cell, which, including flight altitude, equates to 1000 model parameters.

After the first cell C_1 has been built, the second one C_2 is obtained by iterative nearest-neighbor expansions around one of the points along the outer border of the first cell. The third cell is built from one of the points on the outer border of either the first cell, or of the second cell, and so on, until the last cell C_q, so that each sounding in the data sets is assigned to a cell (see Figure 4a). Each cell C_p is described by the location of the t soundings it contains: $S_1^p, S_2^p, \ldots, S_t^p$ (with t not being the same for each cell) and by the location of the nearest neighbors to each of these soundings: $N_1^1, N_2^1, \ldots, N_l^1$; $N_1^2, N_2^2, \ldots, N_m^2; \ldots; N_1^t, N_2^t, \ldots, N_o^t$.

The last step, which leads to the final cells, involves expanding the cells in Figure 4a around their borders to one more order of nearest neighbors. In this way, we create a double overlap between neighboring cells (see Figure 4b). This is the smallest overlap that ensures a robust migration of model parameter information between cells and that guarantees model parameter continuity across the cells. Because of the overlap between neighboring cells, a given sounding $S_l(x,y)$ might be included in more than one cell.

The mechanism of information migration across cells is described in detail in the next section. Note the irregular shapes of the cells. Such irregularity is dictated by the spatial distribution of the soundings, which governs the Delaunay triangles and therefore the nearest neighbors. This cell-building procedure is completely automatic and only requires that the user input the approximate number of data points per cell desired. Ultimately, implementation of the Delaunay triangulation allows selecting, for parallel computation, geometrically unbiased subsets of data that adapt automatically to data-density variations.

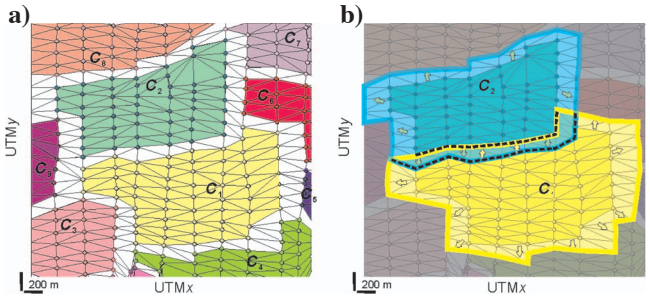

Figure 4. Two stages of production of cells, identified by different colors, for a portion of the Stevenstrup data set. (b) Overlap between neighboring final cells. The dashed line defines the overlap region between the cells C_1 and C_2.

The total number of cells is divided into as many CPUs as are available, and the SCI is run in parallel. Whenever a single sounding S_l belongs to an overlap region, it is inverted more than once. The output of a model parameter for that sounding is the average of the values of the model parameters obtained from the SCI of the individual cells, weighed inversely by their standard deviation. The standard deviation is obtained from the analysis of the model parameter sensitivity resulting from the first inversion run.

Let us consider the case of S_l belonging to n cells. The output for the resistivity of the kth layer is

$$\rho^k(S_l) = \exp\left(\frac{\sum_{i=1}^{n} \frac{\log(\rho_i^k)}{\log(1/(1 + \mathrm{STD}(\rho^k)_i))^2}}{\sum_{i=1}^{n} \left(\frac{1}{1 + \mathrm{STD}(\rho^k)_i}\right)^2}\right). \quad (13)$$

The output for the thicknesses is computed in the same way, and from there, the depths. Using the outcome of the sensitivity analysis of the model parameters in the averaging ensures that well-resolved parameters have a bigger influence on the result. In particular, it ensures that a well-resolved conductance that depends on consistency between layer thickness and conductivity is also well preserved. The output for the sensitivity analysis of each model parameter will be the square root sum of the individual standard deviations. For example,

$$\mathrm{STD}(\rho^k) = \sqrt{\sum_{i=1}^{n} (\mathrm{STD}(\rho^k)_i)^2}. \quad (14)$$

Preserving continuity across subsets with the second inversion run

The results of the first run are used as starting models for the second run, reducing the computation time significantly (to less than half) with respect to the first run. In the overlap zone, the starting models are produced as described in equation 13 and therefore contain information from adjacent cells.

Along the inner edge of the overlapping region (see Figure 5), the results of the first run are used not only as starting models but also as a priori information on the model parameters (i.e., starting model with model confidence given by equation 14). We only apply a priori information to the soundings that lie along the inner edge because

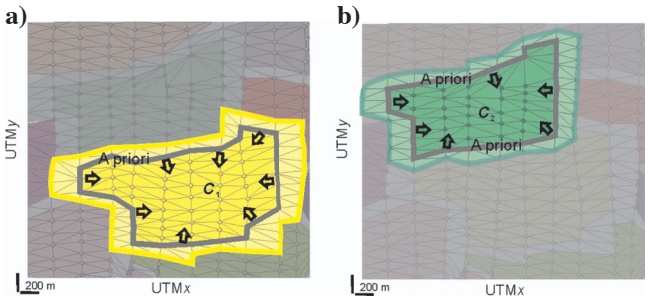

Figure 5. For the SCI of cells (a) C_1 and (b) C_2, all the soundings are started with model parameters obtained from the previous run. The thick gray lines connect the soundings that also use the a priori information from the previous run. The arrows show how the a priori information migrates toward the middle of the cells.

they have all their nearest neighbors included in the cell, as opposed to the soundings along the outer edge. This ensures that the a priori information spreads, through the constraints, as homogeneously as possible, both within and between cells.

Using the results of the first inversion run as starting models for the second run allows model parameter information to be passed, by means of the constraints, between neighboring cells. This ensures, at least to a first-order approximation, a continuous flow of information between soundings, independently of the cells.

SCIs of each cell are once again run in parallel. This time, the final output for the overlapping zones is obtained by keeping the results obtained from the inner edge of the overlapping zone of each cell.

FIELD EXAMPLE

SCI can be applied to all data types for which a 1D forward solution exists. In this article, we cover the case of airborne TEM soundings. Over the past few years, the helicopter borne SkyTEM system

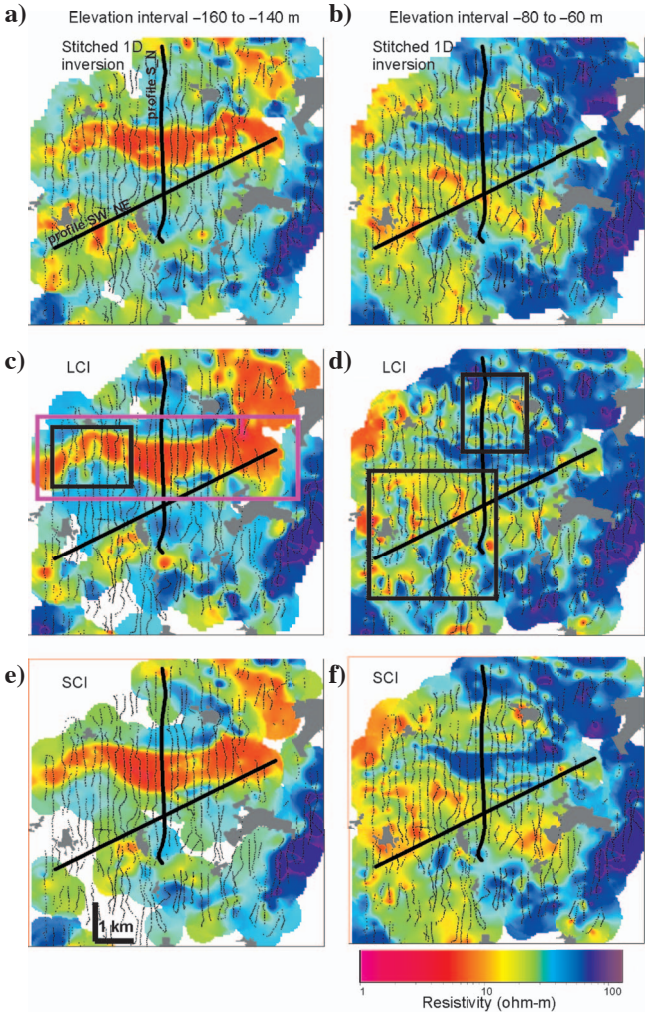

Figure 6. Mean resistivity maps at elevation intervals −160 to −140 m and −80 to −60 m for a portion of the Stevenstrup data set: (a, b) stitched 1D inversion, (c, d) LCI, (e, f) SCI. Black dots represent SkyTEM soundings; black lines represent the profiles shown in Figures 7 and 8. The purple rectangle is the area of the buried valley.

(Sørensen and Auken, 2004) has collected many thousands of kilometers of TEM data, many of them in sedimentary environments for groundwater exploration. We present a case study from an 80-km^2 survey in the Stevnstrup area, eastern Jutland, Denmark, as shown in Figure 2a. Each black dot represents a sounding, which is either a low-moment or a high-moment sounding. The average spacing between flight lines is 250 m. Many soundings near roads and power lines have been removed because of transmitter-induced couplings to power lines and to cables buried along the roads (Danielsen et al., 2003). The full data set contains 5477 soundings. Of these, approximately half are high-moment ($\approx$60,000 Am^2) and the other half low-moment ($\approx$10,000 Am^2) soundings.

In general terms, the geology of the survey area consists of Danien Limestone at the bottom. The limestone is saturated with residual saltwater (with an average resistivity of $\leq$2 ohm m) in the very deep parts and infiltrating freshwater (30–100 ohm-m) in the more superficial parts. On top of this is 0–100 m of heavy Paleogene clay with an average resistivity of 2–5 ohm-m. The uppermost part of the sequence is till, consisting of varying clay mineral content and glacial sands. It was expected that one or more buried valleys were incised into the Paleogene clay. These valleys are filled with outwash sand and gravel (50–80 ohm-m) and represent important aquifer structures (Auken et al., 2003; Jørgensen et al., 2003).

We compare the results of three different inversion approaches: (1) stitched-together independent 1D inversion of individual soundings, (2) LCI, and (3) SCI. Each inversion has the same starting models (in this case, a uniform half-space of 50 ohm-m) and five layers. The number of layers was chosen as the least number of layers that fitted the data while being indicative of the main expected geologic units of the area. The only effect of reducing (increasing) the number of layers would be to increase (reduce) the optimal number of soundings of the SCI cells for computation purposes (always aiming at about 1000 model parameters per cell). As SCI is a parallel procedure, the total inversion time depends on the number of available processors.

First, we present the results in the form of mean resistivity values at different elevation intervals (Figure 6) and then in the form of profiles (Figure 7). The average resistivity maps, at both elevation intervals, clearly demonstrate the effect of the constraints. LCI (Figure 6c and d) promotes along-line continuity, with respect to the stitched-together single-site inversion. For example, note the area that delimits a buried valley that runs in east-west (delimited by the purple rectangle in Figure 6c). However, LCI also introduces elongated features coincident to the flight lines (more evident in the areas delimited by the black rectangles in Figure 6c and d). SCI, on the other hand, produces smooth variations in every direction. It clearly delineates the borders of the buried valley. It resolves continuous west-east features, especially noticeable in the region of the valley, that are not so well identified by the other two methods.

The good conductor present at depth in the valley (Figure 6e) represents residual saline water in a limestone host, whereas the shallower resistive structure visible in Figure 6f corresponds to unconsolidated sediments. Figure 7d shows a sketch of the vertical section of the geology of the area.

The complete SCI was conducted on the data set more than once, with different starting points for the creation of cells, which therefore had different locations, shapes, and sizes. The results, not shown here, proved that SCI is robust with respect to the choice of the starting point (i.e., of the cell's geometry).

Figures 7 and 8 show the cross sections of the two profiles drawn onto the maps in Figure 6. The two profiles allow comparison of the results of the inversion methodologies along different directions. In both, the single-site stitched-together inversion gives the least lateral continuity, as expected. The south-north profile in Figure 7 follows a flight line and therefore also the chain of soundings constrained in the LCI. This should produce good results, apart from possible minor distortions from 2D effects along the edges of the buried valley. A sketch of the geological cross section inferred from available geologic models is shown in Figure 7d. Both the LCI and the SCI correctly identify all of the main geologic units. The single-site inversion fails to delineate the boundary between clay and limestone recorded in the proximity of the borehole, although it does define the boundary in other areas of the profile.

The minor difference between SCI and LCI is in the detection of the whole clay-limestone boundary in the northern portion of the profile, which SCI defines more continuously. This result is because the constraints set in SCI allow model parameter information to migrate across the flight path, not only along it (as in LCI). Therefore, model parameters are, better resolved. We will return to the parameter sensitivity analysis issue at the end of this section.

In Figure 7, black bold arrows indicate the location of the main discrepancies between the results of the SCI and the other methods. In the portions of the profile where the limestone is overlain by a thick clay cover, its absolute resistivity values are underestimated. The thick clay layer also masks the presence of deeper residual saltwater.

Figure 8 displays less continuity because the direction of the southwest-northeast profile does not coincide with flight lines and thus has a lower sounding density. Both SCI and LCI results agree substantially with the available geologic model (Figure 8d). SCI, however, provides more continuous results overall, both at the boundary between the shallow resistive layers of glacial sediments and clay and at depth along the clay-limestone boundary. Black bold arrows indicate once again the main differences between the SCI and the other two methods.

So far, we have shown that SCI reveals the same overall geologic structures as LCI but that they are significantly different in detail. SCI recovers the actual geology of the area better, and the pictures are much more coherent compared to those based on profile-oriented LCI and the individual soundings inversions. We now analyze the model parameter covariance and the data-fit residual to give a mathematical evaluation of the results produced.

The spatial maps in Figure 9a and b show the standard deviation factor for the resistivity of layer 3 for the LCI and for the SCI, respectively. Moderately to well-determined parameters have a standard deviation factor less than 1.5; a standard deviation factor greater than two corresponds to unresolved parameters (Auken and Christiansen, 2004). In SCI, more model parameter information is passed between soundings than in LCI. This decreases the uncertainty of the model parameters, which benefit from the across-line constraints. The lower standard deviation factor of Figure 9b suggests that a significant amount of model parameter information in the SCI has migrated across the direction of flight lines, allowing better resolution of model parameters.

The question arises whether the better model parameter resolution comes at the cost of a worse fit to the data for the SCI because of the smoother model space. The white and black dots in Figure 9 represent, respectively, fitted and unfitted data (residual lower or higher

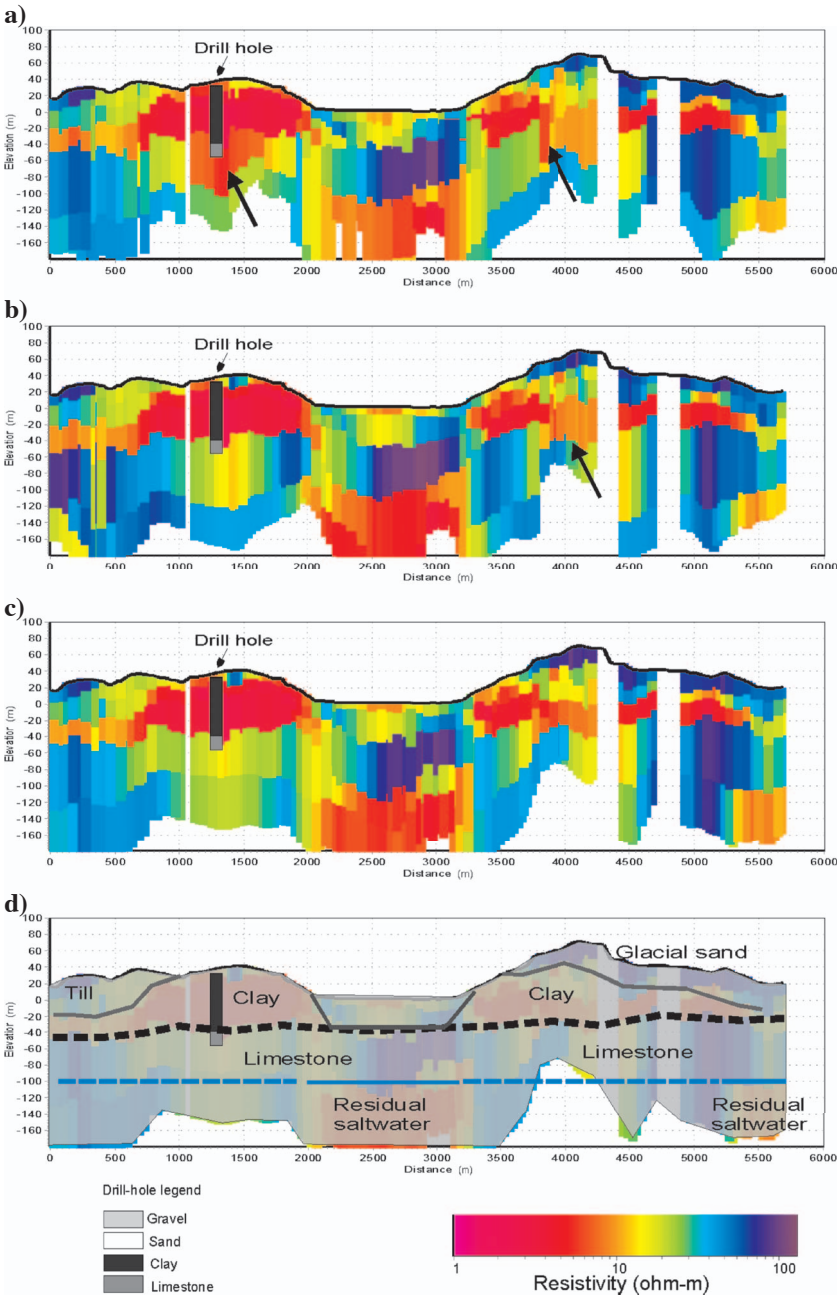

Figure 7. Resistivity cross section for south-north profile: (a) stitched-together single-site inversion, (b) LCI, (c) SCI, (d) sketch of geology cross section.

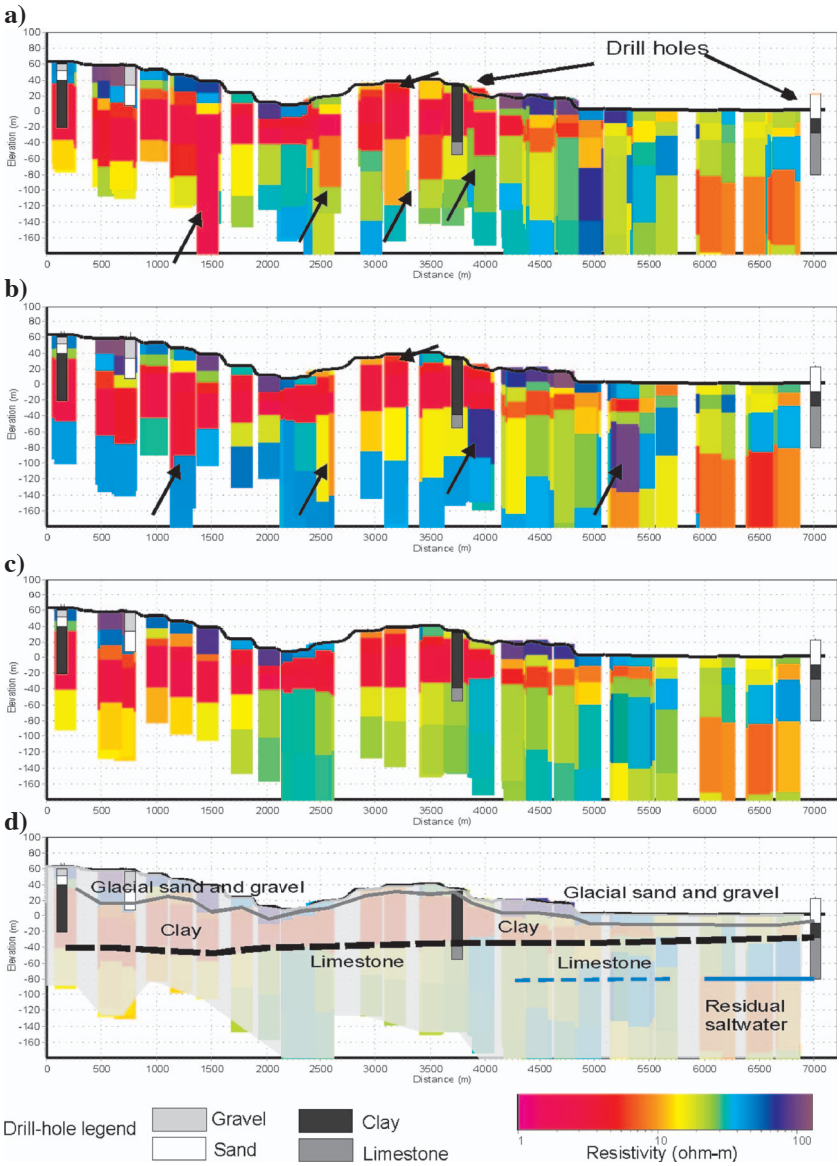

Figure 8. Resistivity cross section for the southwest-northeast profile: (a) stitched-together single-site inversion, (b) LCI, (c) SCI, (d) sketch of geology cross section.

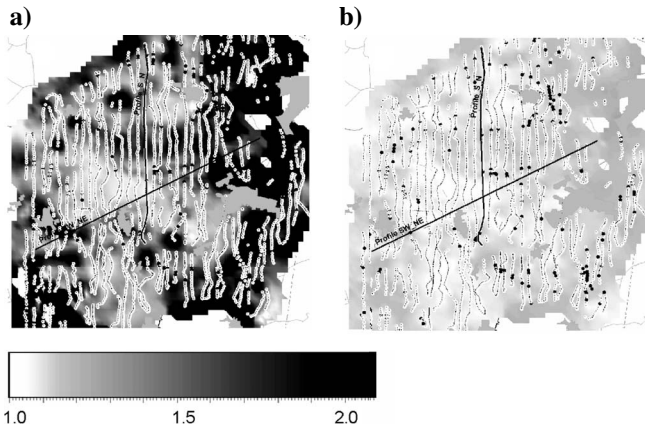

Figure 9. Layer 3, standard deviation factor of resistivity of third layer in (a) LCI and (b) SCI. The white and black dots represent, respectively, data that were fitted or not fitted within the noise level by the inversions.

than one standard deviation of the stacked $-dB/dt$ signal). Their density shows that this is not the case. The LCI and the SCI fit the data in 96% and 95% of the total number of soundings, respectively. Therefore, we conclude the SCI decreases the uncertainty of model parameters while fitting the data.

The mean resistivity slice map, the profiles, the sensitivity analysis of the model parameters, and the analysis of the data fit prove that, overall, SCI fits the data and produces well-determined output models that resemble the known geology of the area better than stitched-together original inversions and also better than a profile-oriented inversion methodology such as LCI.

DISCUSSION AND OTHER APPLICATIONS

The SCI concept is applicable to different geophysical data types distributed on a plane. The Delaunay triangulation ensures an efficient connection of data points with very irregular data density. Thus, SCI could be applied to a combination of similar data sets coming from methodologies with different data-sampling densities, such as galvanic (surface or downhole) and TEM or HEM measurements. Despite the 1D forward approximation, SCI can also be applied with success to geologic settings that present modest 2D and 3D variations because the strength of the constraints can be adjusted to reflect the geologic variability of the area. Even though SCI is not designed for a single profile of data, it would be applicable to it, effectively reducing to the LCI method.

SCI has the potential to be particularly effective in fixed-wing airborne EM (AEM) data. These systems, where the receiver is towed in a bird behind and below the transmitter, are asymmetric and produce flight-direction-dependent asymmetries. That is, the model parameters (e.g., average resistivity maps) obtained from processing data flown along a line in one direction differ significantly from those obtained with data from the same line but flown in the opposite direction (Smith and Chouteau, 2006). Because adjacent lines typically are flown in opposite directions, such asymmetries are usually removed from maps by applying spatial filters, using perpendicular tie lines, or interpolating reverse line-direction data from adjacent lines (Smith and Chouteau, 2006). The advantage of the SCI approach is that, rather than being filtered or interpolated, information is passed across adjacent flight lines and used to increase model parameter resolution.

Even when using a nonspecialized spare matrix operation such as in the present implementation, there is no inherent limit on the dimension of the data sets that can be inverted with SCI. Larger data sets increase the number of cells and therefore slow down the completion of the SCI process (or require more parallel processes). However, dividing the data set into subsets allows SCI to be applied to arbitrarily large data sets. Applying specialized sparse matrix opera-

tions, the subject of ongoing work, will largely increase the size of the cells.

CONCLUSIONS

SCI applies horizontal constraints for ensuring lateral continuity, improving resolution of model parameters for single stations that are not well resolved by the data from that station alone. Use of Delaunay triangulation for the constraints allows SCI to adapt efficiently to data-density variations. In profile-oriented data sets, it ensures a connection between adjacent lines by means of across-line constraints. Therefore, it eliminates the common elongated features that often coincide with the direction of the survey (i.e., flight lines) and that distort the continuity of geologic units across flight lines. Although based on a 1D forward model, SCI results in a computationally practical, quasi-3D inversion of EM data.

SCI can be applied to different data types. In the study presented here, SCI was applied successfully to quasi-3D modeling of TEM data in a sedimentary environment. It produced laterally smooth, well-determined results that are more geologically reasonable than individual sounding inversions or the profile-oriented LCI. The SCI allowed a significant improvement in the mapping of the intermediate clay-limestone interface.

ACKNOWLEDGMENTS

The authors would like to thank the County of Aarhus for permission to use the Stevnstrup data set and for numerous discussions on the output with Sine Rasmussen and Verner Søndergaard. We also thank Joakim Westergaard (from the hydrogeophysics group of the University of Aarhus), who was partly responsible for reprocessing the data prior to our experiments, and associate professor Niels Christensen for numerous comments and enhancements of this manuscript. Also, comments from the reviewers greatly increased the readability of this manuscript. This work was funded by the County of Aarhus, County of Vejle, and HGG.

REFERENCES

Auken, E., and A. V. Christiansen, 2004, Layered and laterally constrained 2D inversion of resistivity data: Geophysics, **69**, 752–761.

Auken, E., A. V. Christiansen, B. H. Jacobsen, N. Foged, and K. I. Sørensen, 2005a, Piecewise 1D laterally constrained inversion of resistivity data: Geophysical Prospecting, **53**, 497–506.

Auken, E., A. V. Christiansen, L. Jacobsen, and K. I. Sørensen, 2005b, Laterally constrained 1D inversion of 3D TEM data: Symposium on the Application of Geophysics to Engineering and Environmental Problems (SAGEEP) Proceedings, 519–524.

Auken, E., F. Jørgensen, and K. I. Sørensen, 2003, Large-scale TEM investigation for groundwater: Exploration Geophysics, **33**, 188–194.

Aurenhammer, F., 1991, Voronoi diagrams — A survey of a fundamental geometric data structure: ACM Computing Surveys, **23**, 345–405.

Barber, B., D. Dobkin, and H. Huhdanpaa, 1996, The Quickhull algorithm for convex hulls: ACM Transactions on Mathematical Software, **22**, 469–483.

Bohm, G., P. Galuppo, and A. Vesnaver, 2000, 3D adaptive tomography using Delaunay triangles and Voronoi polygons: Geophysical Prospecting, **48**, 723–744.

Brodie, R., and M. Sambridge, 2006, A holistic approach to inversion of frequency-domain airborne EM data: Geophysics, **71**, no. 6, G301–G312.

Danielsen, J. E., E. Auken, F. Jørgensen, V. H. Søndergaard, and K. I. Sørensen, 2003, The application of the transient electromagnetic method in hydrogeophysical surveys: Journal of Applied Geophysics, **53**, 181–198.

Effersø, F., E. Auken, and K. I. Sørensen, 1999, Inversion of band-limited TEM responses: Geophysical Prospecting, **47**, 551–564.

Gyulai, A., and T. Ormos, 1999, A new procedure for the interpretation of VES data, 1.5-D simultaneous inversion method: Journal of Applied Geophysics, **41**, 1–17.

Huang, H., and D. C. Fraser, 2003, Inversion of helicopter electromagnetic data to a magnetic conductive layered earth: Geophysics, **68**, 1211–1223.

Jørgensen, F., H. Lykke-Andersen, P. Sandersen, E. Auken, and E. Nørmark, 2003, Geophysical investigations of buried Quaternary valleys in Denmark: An integrated application of transient electromagnetic soundings, reflection seismic surveys and exploratory drillings: Journal of Applied Geophysics, **53**, 215–228.

Macnae, J., and Y. Lamontagne, 1987, Imaging quasi-layered conductive structures by simple processing of transient electromagnetic data: Geophysics, **52**, 545–554.

Mansoor, N., L. Slater, F. Artigas, and E. Auken, 2006, High-resolution geophysical characterization of shallow-water wetlands: Geophysics, **71**, no. 4, B101–B109.

Newman, G. A., W. L. Anderson, and G. W. Hohmann, 1987, Interpretation of transient electromagnetic soundings over three-dimensional structures for the central-loop configuration: Geophysical Journal of the Royal Astronomical Society, **89**, 889–914.

Sambridge, M., 1999, Geophysical inversion with a neighourhood algorithm — I, Searching a parameter space: Geophysical Journal International, **138**, 479–494.

Sambridge, M., J. Braun, and H. McQueen, 1995, Geophysical parametrization and interpolation of irregular data using natural neighbours: Geophysical Journal International, **122**, 837–857.

Santos, F. A. M., 2004, 1-D laterally constrained inversion of EM34 profiling data: Journal of Applied Geophysics, **56**, 123–134.

Sengpiel, K. P., and B. Siemon, 2000, Advanced inversion methods for airborne electromagnetic exploration: Geophysics, **65**, 1983–1992.

Smith, R. S., and M. C. Chouteau, 2006, Combining airborne electromagnetic data from alternating flight directions to form a virtual symmetric array: Geophysics, **71**, no. 2, G35–G41.

Sørensen, K. I., and E. Auken, 2004, SkyTEM — A new high-resolution helicopter transient electromagnetic system: Exploration Geophysics, **35**, 191–199.

Ward, S. H., and G. W. Hohmann, 1988, Electromagnetic theory for geophysical applications, *in* M. N. Nabighian, ed., Electromagnetic methods in applied geophysics: SEG, 131–311.

Xue, Y., M. Sun, and A. Ma, 2004, On the reconstruction of three-dimensional complex geological objects using Delaunay triangulation: Future Generation Computer Systems, **20**, 1227–1234.